The optimized electrochemical deposition of bismuth-bismuth telluride layered crystal structures

The optimized electrochemical deposition of bismuth-bismuth telluride layered crystal structures

Aliaksei Bakavets[1], Yauhen Aniskevich[2], Genady Ragoisha[1], Natalia Tsyntsaru[3,4], Henrikas Cesiulis[3,5], Eugene Streltsov[2]

[1]Research Institute for Physical Chemical Problems, Belarusian State University, Minsk, Belarus
[2]Faculty of Chemistry, Belarusian State University, Minsk, Belarus
[3]Vilnius University, Faculty of Chemistry and Geosciences, Vilnius, Lithuania
[4]Institute of Applied Physics, Chisinau, Moldova
[5]JSC Elektronikos Perdirbimo Technologijos, Vilnius, Lithuania

E-mail: alexeibokovets@gmail.com

Abstract. Underpotential deposition, i.e. the cathodic deposition above reversible potential E(Me^{n+}/Me), produces an atomic layer of a metal on a semiconductor electrode, such as e.g. bismuth telluride. This phenomenon allows electrodeposition of superlattices formed of building blocks of a layered semiconductor structure joined by biatomic metal interlayer. This work outlines the optimized pulse potential controlled electrodeposition of $(Bi_2)_m(Bi_2Te_3)_n$ films produced under mentioned above technique. The influence on the morphology of the electrodeposited films of key-parameters as applied pulse frequency, duty cycle, a routine of sodium dodecyl sulfate introduction in the electrolyte is discussed. The optimized procedure comprises a short (about 10 s) cathodic pre-treatment at high overpotential of the cathodic reaction, the subsequent periodic switching for 120 min between potentials of electrodeposition and refinement at 0.1 Hz and 5% duty cycle with addition of surfactant 60 min after the start of the electrodeposition.

1. Introduction

Nanostructures formed by an alteration of ultra-thin layers of a semiconductor and a metal are of the interest for various applications and are especially promising for the development of new thermoelectric materials [1-4]. The major characteristic of a thermoelectric material efficiency, its figure of merit, depends on ratio of electric and thermal conductivities. Variations of the two latter characteristics are coupled in usual materials and the main route to thermoelectric materials with low thermal conductivity uncoupled from electric conductivity implies application of nanostructures [5]. This stimulates much work on nanostructuring of bismuth telluride, one of the best thermoelectric materials at room temperature [6-8], including investigation of Bi_2Te_3 nanoparticles electrodeposition [9-20]. Superlattices of $(Bi_2)_m(Bi_2Te_3)_n$ series formed by alteration of Te-Bi-Te-Bi-Te quintuples and bismuth biatomic layers [1-3, 21-27] and similar $(Bi_2)_m(Bi_2Se_3)_n$ [28-32] and $(Sb_2)_m(Sb_2Te_3)_n$ [33] layered materials are especially attractive as their specific structure which determines low thermal conductivity [1, 2, 22, 24, 31] is characteristic of ordinary crystalline state, not only nanoparticles. We have presented recently [3] the electrochemical approach for such superlattice formation by in situ

insertion of metal interlayers into semiconductor layered crystal structure during the semiconductor pulsed electrodeposition.

The prerequisites of the technique are the layered crystal structure of a semiconductor, such as of bismuth telluride crystal which is formed by stacks of Te-Bi-Te-Bi-Te quintuples joined by weak van der Waals bonds, and the capacity of given semiconductor to acquire metal adlayer on its surface above the reversible potential $E(Me^{n+}/Me_{bulk})$ of the corresponding bulk metal. The latter phenomenon, i.e. the underpotential deposition (upd) of metal adlayer on a semiconductor, has been reviewed lately in [34], electrochemical properties of metal monolayers (adlayers) on bismuth telluride were reported in [35, 36].

The goal of this work was the optimization of parameters of $(Bi_2)_m(Bi_2Te_3)_n$ pulse potential controlled electrodeposition for preparation of compact uniform films with monitoring of the electrodeposition by scanning electron microscopy (SEM). The scope of the experiment in this work was limited to the investigation of parameters of the pulsed electrodeposition effect on morphology in the electrodeposition of $(Bi_2)_m(Bi_2Te_3)_n$ films, as the proof of $(Bi_2)_m(Bi_2Te_3)_n$ formation at the condition of our experiments was obtained earlier [3] by numerous experimental and theoretical methods.

2. Experimental

Electrodeposition of $(Bi_2)_m(Bi_2Te_3)_n$ films was performed in a three-electrode cell with stainless steel foil as a working electrode, Ag|AgCl|KCl(sat) reference electrode, and Pt counter electrode. Pulse potential control was provided by Gamry Series 300 potentiostat. The morphology of the films in the electrodeposition was monitored using Hitachi TM3000 Tabletop microscope. Substrates were subsequently rinsed in the hot nitric acid, polished with 0.05 μm alumina suspension, and electrochemically treated by cyclic polarization in the potential range between –0.4 V and 0.8 V in 3M HNO_3 solution. The electroactive area was isolated from the rest of the electrode by acid-resistant varnish. Additional experimental details of $(Bi_2)_m(Bi_2Te_3)_n$ electrodeposition were presented in [3].

Bismuth adlayer (Bi_{ad}) is electrodeposited onto bismuth telluride in the electrode potentials region of bulk bismuth anodic oxidation above $E(Bi^{3+}/Bi)$ (figure 1). Thus, the electrodeposition of bismuth adlayer on Bi_2Te_3 is efficiently prevented from nucleation and growth of Bi metallic phase by the potential control. Bismuth telluride electrodeposition proceeds in a more negative electrode potential region concurrently with bulk bismuth electrodeposition. In order to enable alternating deposition of Te-Bi-Te-Bi-Te quintuples and Bi_{ad} with exclusion of metallic bismuth, the potential is alternatively switched between the both regions (figure 2). The two bismuth adlayers thus formed on adjacent Te-Bi-Te-Bi-Te quintuples combine into a bismuth bilayer, which results in the electrochemical formation of $(Bi_2)_m(Bi_2Te_3)_n$ superlattice structure [3], in which bismuth bilayers occupy places at van der Waals planes between quintuples of bismuth telluride structure. The *m : n* ratio in the superlattice structure was controlled in [3] by the concentrations of bismuth and tellurium precursors in the electrolyte, $Bi(NO_3)_3$ and TeO_2 dissolved in an aqueous HNO_3 solution.

Parameters of the pulse electrodeposition were varied in each experiment. In the original procedure, each electrode was pretreated at −400 mV for 10 seconds in the electrolyte containing 8.75 mM $Bi(NO_3)_3$, 1.25 mM TeO_2, 1 M HNO_3, then the electrodeposition with rectangular wave pulse potential control at 1.0 Hz pulse frequency (*f*) and 10% pulse duty cycle (γ) was carried out for 30 minutes. The duty cycle is the fraction of each period attributed to the active electrodeposition stage. The cathodic pre-treatment stage was found to facilitate uniformity in the subsequent electrodeposition. The nucleation of bismuth telluride on the bare substrate proceeds at high overpotential during the cathodic pre-treatment stage, thus providing uniform coverage of the electrode surface by centers for the following active electrodeposition stage. The potential of active electrodeposition, E_{dep} in the region of Bi_2Te_3 electrodeposition, and also the refinement potential, E_{ref} in the region of bulk bismuth anodic oxidation and Bi_{ad} cathodic deposition (figure 2) were determined from cyclic voltammetry and were set to –100 mV and 60 mV respectively for 8.75 mM $Bi(NO_3)_3$,

1.25 mM TeO_2, 1 M HNO_3 electrolyte composition. Sodium dodecyl sulfate (SDS) was used as a surfactant.

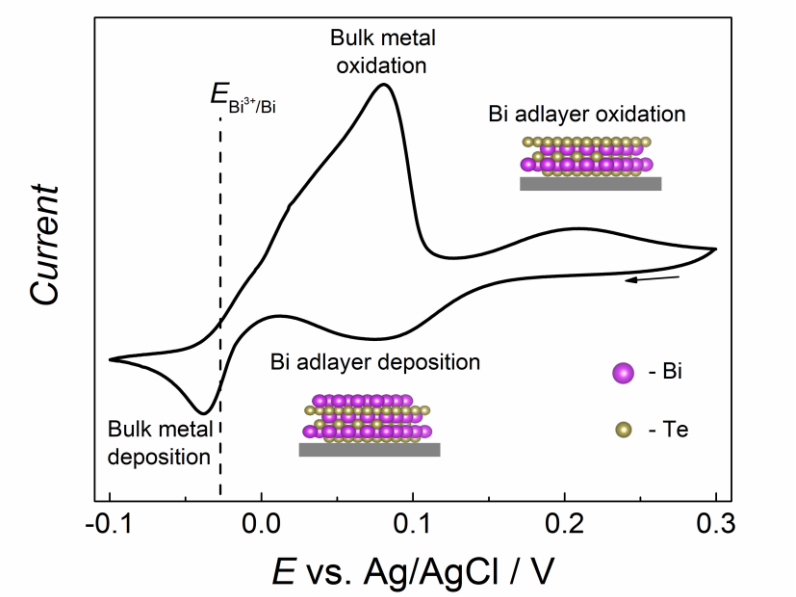

Figure 1. Cyclic voltammogram of Bi_2Te_3 electrode in 10 mM $Bi(NO_3)_3$, 1 M HNO_3 electrolyte solution.

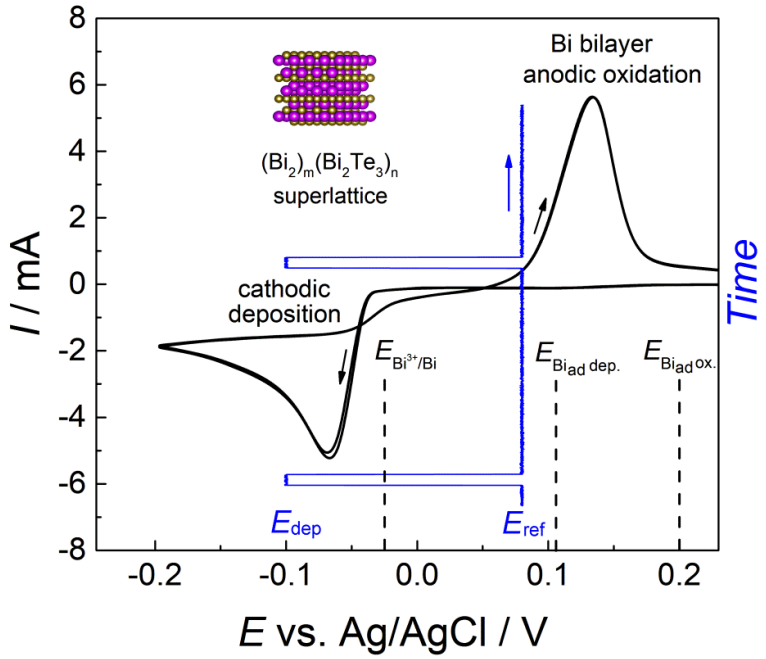

Figure 2. Pulse potential control profile of $(Bi_2)_m(Bi_2Te_3)_n$ electrodeposition (blue pulses) overlaid on a cyclic voltammogram (black) of $(Bi_2)_m(Bi_2Te_3)_n$ electrode on stainless steel substrate in 8.75 mM $Bi(NO_3)_3$, 1.25 mM TeO_2, 1 M HNO_3 electrolyte solution.

In the optimization procedure, γ (in %) was set to 5, 10, 20, 30, 40, 50, and 80, while other parameters were kept constant. Then, the pulse frequency, *f* (in Hz) was varied as 0.1, 0.5, 1.0, 5.0, and 10.0. The lowest frequency was restricted by 0.1 Hz, because of the required alteration of the electrodeposition and refinement stages. In the third optimization step, the time of the cathodic pre-treatment was varied as 10, 30, 60, and 120 seconds. The fourth variable parameter was time of the deposition: the films were deposited for 30, 60, 120, and 240 minutes. In addition, the effect of surfactant (sodium dodecyl sulfate) and the method of its introduction were studied.

3. Results and discussion

3.1 Pulse frequency and duty cycle

Pulse frequency and duty cycle control the time of the electrodeposition and refinement stages of the periodic process, and also replenishment of the electrolyte solution near the working electrode by electroactive species. Pulse frequency and duty cycle influence on the film morphology were studied independently. Figures 3 and 4 summarize the main effects of these parameters variation. A short time of the electrodeposition was used in those series since the formation of non-uniformities can be best observed at early stages.

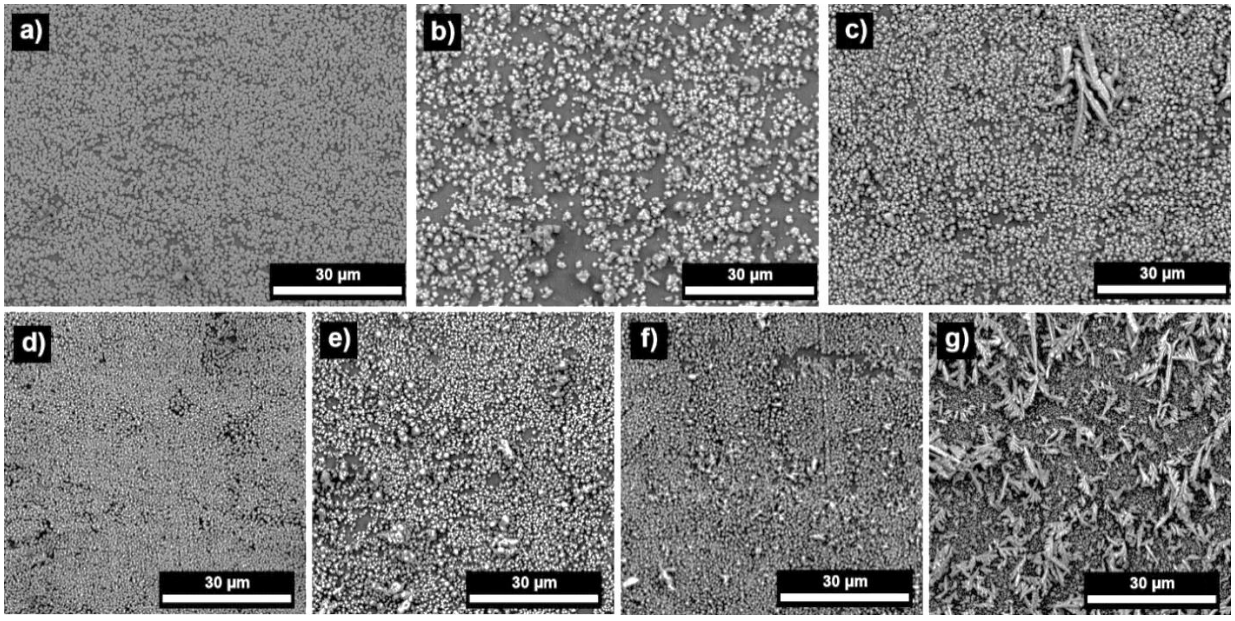

Figure 3. SEM images of $(Bi_2)_m(Bi_2Te_3)_n$ films electrodeposited at various γ (in %): a) 5; b) 10; c) 20; d) 30; e) 40; f) 50; g) 80. Other parameters are: f = 1 Hz, E_{dep} = −100 mV, E_{ref} = 60 mV.

At high duty cycle, the duration of the active electrodeposition stage increases, whereas the time available for diffusion and accumulation of electroactive species near the electrode surface and also the time of refinement stage decrease. As figure 3 shows, short pulses facilitate the formation of uniform films. However, when the pulses were short due to high frequency, the substrate was not uniformly covered by the $(Bi_2)_m(Bi_2Te_3)_n$ particles. Rare pulses favour the deposition of uniform-size crystallites (figure 4).

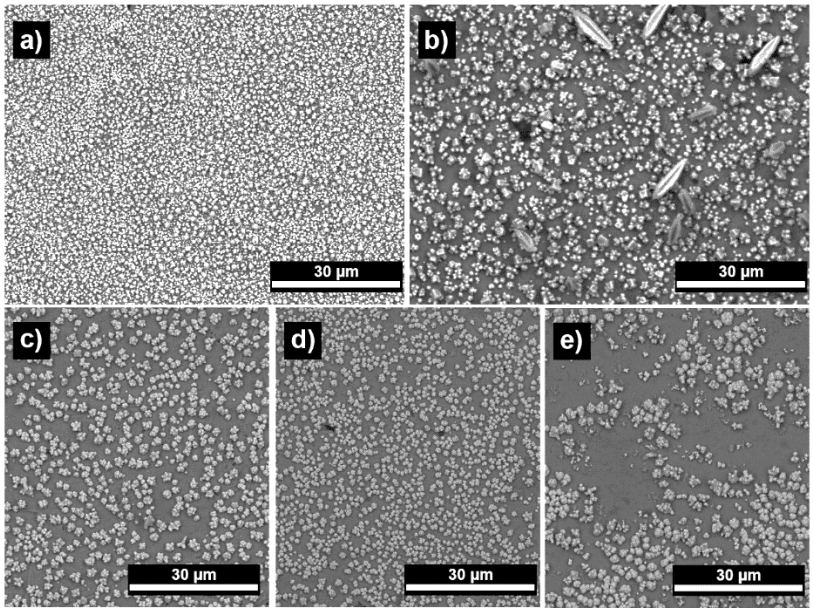

Figure 4. SEM images of $(Bi_2)_m(Bi_2Te_3)_n$ films electrodeposited at various pulse frequencies (in Hz): a) 0.1; b) 0.5; c) 1.0; d) 5.0; e) 10. Other deposition parameters are: γ = 10%, E_{dep} = −100 mV, E_{ref} = 60 mV.

3.2. Surface-active substance

Pulse deposition gives 3 µm thick film at 120 minutes, the thickness was typically sufficient for preparation of flexible thermoelectric devices with dissent thermoelectric parameters in the case of bismuth telluride [37]. However, the $(Bi_2)_m(Bi_2Te_3)_n$ films deposited without surfactant are rough, non-uniform, and porous, due to dendrite growth. In the case of bismuth telluride electrodeposition similar problem was mitigated with the use of sodium lignosulfonate surfactant [38, 39]. SDS has shown good results in our case. Its optimal concentration is approx. 55 mg L^{-1}; below and above this concentration the film roughness and formation of non-uniformly sized crystallites increases (figure 5).

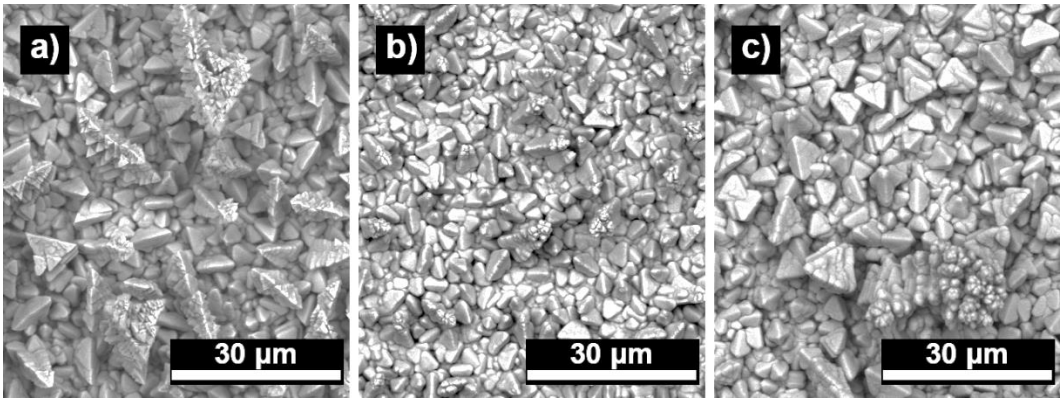

Figure 5. SEM images of $(Bi_2)_m(Bi_2Te_3)_n$ films electrodeposited at various SDS concentrations (in mg L^{-1}) in the electrolyte: a) 40; b) 55; c) 70. Other deposition parameters are: f = 0.1 Hz, γ = 5%, E_{dep} = −100 mV, E_{ref} = 60 mV.

The films electrodeposited from the acidic solution have originally poor adhesion to the stainless steel substrate. The addition of a surface-active agent at the beginning of the deposition process reduces the adhesion even greater and hinders the formation of the uniform film so that only rare agglomerates are formed (figures 6a and 6b). The solution of this problem consists in the addition of surfactant after the

nucleation stage, when the film covers the electrode with the first layer of crystallites. The addition of the surfactant at this stage has provided the formation of a very compact uniform film with tapered crystallite shape morphology (figure 6c).

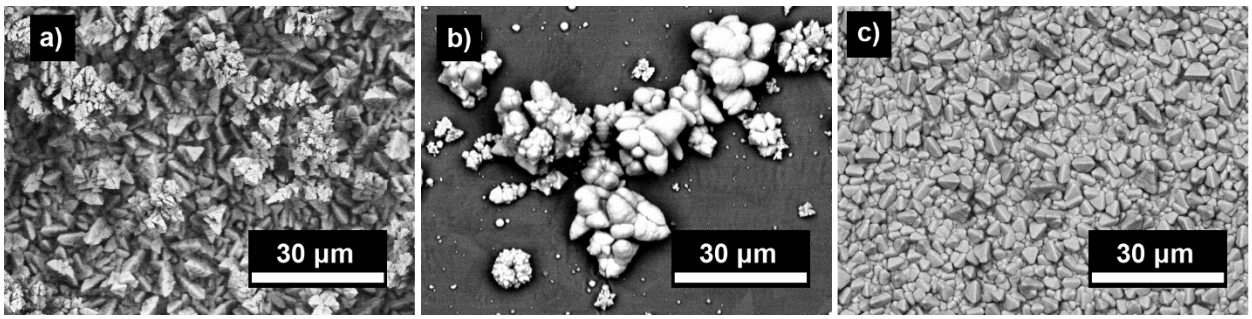

Figure 6. SEM images of $(Bi_2)_m(Bi_2Te_3)_n$ films electrodeposited: a) without SDS; b) with SDS added at the beginning of the deposition; c) with SDS added 60 min. after the start of the deposition. Other deposition parameters: f = 0.1 Hz, γ = 5%, E_{dep} = −100 mV, E_{ref} = 60 mV.

Conclusion

The role of pulse frequency, duty cycle, cathodic pre-treatment and the way of SDS introduction in the electrolyte as factors affecting the morphology in the periodic pulse potential controlled electrodeposition of $(Bi_2)_m(Bi_2Te_3)_n$ films was investigated. The optimized procedure for the electrodeposition of compact films should include:

1) the short (about 10 s) cathodic pre-treatment at high overpotential of the cathodic reaction;
2) the subsequent periodic switching for 120 min of the potential between −100 mV and 60 mV at f = 0.1 Hz and γ = 5% in the active electrodeposition stage;
3) the surfactant addition after 60 min from the beginning of the electrodeposition.

Acknowledgments

Authors acknowledge funding from H2020 project MSCA-RISE-2017-778357-SMARTELECTRODES.

References

[1] Bos J W G, Zandbergen H W, Lee M-H, Ong N P and Cava R J 2007 *Phys. Rev.* B **75** 195203.
[2] Sharma P A, Lima Sharma A L, Medlin D L, Morales A M, Yang N, Barney M, He J, Drymiotis F, Turner J and Tritt T M 2011 *Phys. Rev.* B **83** 235209.
[3] Bakavets A, Aniskevich Y, Yakimenko O, Jo J H, Vernickaite E, Tsyntsaru N, Cesiulis H, Kuo L-Y, Kaghazchi P, Ragoisha G, Myung S-T and Streltsov E 2020 *J. Power Sources* **450** 227605.
[4] Termentzidis K, Pokropyvnyy O, Woda M, Xiong S, Chumakov Y, Cortona P and Volz S 2013 *J. Appl. Phys.* **113** 013506.
[5] Biswas K, He J, Blum I D, Wu C I, Hogan T P, Seidman D N, Dravid V P and Kanatzidis M G 2012 *Nature* **489** 414-8.
[6] Dresselhaus M S, Chen G, Tang M Y, Yang R, Lee H, Wang D, Ren Z, Fleurial J P and Gogna P 2007 *Adv. Mater.* **19** 1043–53.
[7] Heremans J P, Dresselhaus M S, Bell L E and Morelli D T 2013 *Nat. Nanotechnol.* **8** 471–3.
[8] Mamur H, Bhuiyan M R A, Korkmaz F and Nil M 2018 *Renew. Sustain. Energy Rev.* **82** 4159–69.
[9] Pinisetty D, Davis D, Podlaha-Murphy E J, Murphy M C, Karki A B, Young D P and Devireddy R V 2011 *Acta Materialia* **59** 2455–61.

[10] Prieto A L, Sander M S, Martin-Gonzalez M S, Gronsky R, Sands T and Stacy A M 2001 *J. Am. Chem. Soc.* **123** 7160–1.
[11] Sander M S, Gronsky R, Sands T and Stacy A M 2002 *Chem. Mater.* **15** 335–9.
[12] Menke E J, Li Q and Penner R M 2004 *Nano Lett.* **4** 2009–14.
[13] Yu H, Gibbons P C and Buhro W E 2004 *J. Mater. Chem.* **14** 595–602.
[14] Jin C, Xiang X, Jia C, Liu W, Cai W, Yao L and Li X 2004 *J. Phys. Chem.* B **108** 1844–7.
[15] Zhou J, Jin C, Seol J H, Li X and Shi L 2005 *Appl. Phys. Lett.* **87** 133109.
[16] Lee J, Farhangfar S, Lee J, Cagnon L, Scholz R, Gösele U and Nielsch K 2008 *Nanotechnology* **19** 365701.
[17] Mavrokefalos A, Moore A L, Pettes M T, Shi L, Wang W and Li X 2009 *J. Appl. Phys.* **105** 104318.
[18] Bejenari I, Kantser V and Balandin A A 2010 *Phys. Rev.* B **81** 075316.
[19] Frantz C, Stein N, Gravier L, Granville S and Boulanger C 2010 *J. Electron. Mater.* **39** 2043–8.
[20] Frantz C, Stein N, Zhang Y, Bouzy E, Picht O, Toimil-Molares M E and Boulanger C 2012 *Electrochim. Acta* **69** 30–7.
[21] Bos J W G, Faucheux F, Downie R A and Marcinkova A 2012 *J. Solid State Chem.* **193** 13–8.
[22] Thakur V, Upadhyay K, Kaur R, Goyal N and Gautam S 2020 *Mater. Today Adv.* **8** 100082.
[23] Concepción O, Galván-Arellano M, Torres-Costa V, Climent-Font A, Bahena D, Manso Silván M, Escobosa A and De Melo O 2018 *Inorg. Chem.* **57** 10090–9.
[24] Li Bassi A, Bailini A, Casari C S, Donati F, Mantegazza A, Passoni M, Russo V and Bottani C E 2009 *J. Appl. Phys.* **105** 124307.
[25] Eschbach M, Lanius M, Niu C, Młyńczak E, Gospodarič P, Kellner J, Schüffelgen P, Gehlmann M, Döring S, Neumann E, Luysberg M, Mussler G, Plucinski L, Morgenstern M, Grützmacher D, Bihlmayer G, Blügel S and Schneider C M 2017 *Nat. Commun.* **8** 14979.
[26] Chagas T, Ribeiro G A S, Gonçalves P H R, Calil L, Silva W S, Malachias Â, Mazzoni M S C and Magalhães-Paniago R 2020 *Electron. Struct.* **2** 015002.
[27] Stillwell R L, Jenei Z, Weir S T, Vohra Y K and Jeffries J R 2016 *Phys. Rev.* B **93** 094511
[28] Lind H and Lidin S 2003 *Solid State Sci.* **5** 47–57.
[29] Valla T, Ji H, Schoop L M, Weber A P, Pan Z H, Sadowski J T, Vescovo E, Fedorov A V., Caruso A N, Gibson Q D, Müchler L, Felser C and Cava R J 2012 *Phys. Rev.* B **86** 3–7.
[30] Gibson Q D, Schoop L M, Weber A P, Ji H, Nadj-Perge S, Drozdov I K, Beidenkopf H, Sadowski J T, Fedorov A, Yazdani A, Valla T and Cava R J 2013 *Phys. Rev.* B **88** 081108.
[31] Samanta M and Biswas K 2020 *Chem. Mater.* **32** 8819–26.
[32] Lind H, Lidin S and Häussermann U 2005 *Phys. Rev.* B **72** 184101.
[33] Johannsen J C, Autès G, Crepaldi A, Moser S, Casarin B, Cilento F, Zacchigna M, Berger H, Magrez A, Bugnon Ph, Avila J, Asensio M C, Parmigiani F, Yazyev O V and Grioni M 2015 *Phys. Rev.* B **91** 201101.
[34] Ragoisha G A, Aniskevich Y M, Bakavets A S and Streltsov E A 2020 *J. Solid State Electrochem*. **24** 2585–94.
[35] Bakavets A S, Aniskevich Y M, Ragoisha G A and Streltsov E A 2017 *J. Belarusian State Univ. Chem.* **1**(2) 3–13.
[36] Bakavets A S, Aniskevich Y M, Ragoisha G A and Streltsov E A 2018 *Electrochem. Commun.* **94** 23–6.
[37] Na J, Kim Y, Park T, Park C and Kim E 2016 *ACS Appl. Mater. Interfaces* **8** 32392-400.
[38] Caballero-Calero O, Díaz-Chao P, Abad B, Manzano C V, Ynsa M D, Romero J J, Muñoz Rojo M and Martín-González M S, 2014, *Electrochimica Acta* **123** 117-26.
[39] Naylor A J, Koukharenko E, Nandhakumar I S and White N M 2012, *Langmuir* **28** 8296-9.